Insights into Redox Reactions and Ionic Transfers in Nickel/Iron Layered Double Hydroxide in Potassium Hydroxide

Elise Duquesne, Stéphanie Betelu, Cyrille Bazin, Alain Seron, Ioannis Ignatiadis, Hubert Perrot, Ozlem Sel, Catherine Debiemme-Chouvy

Insights into redox reactions and ionic transfers in Ni/Fe layered double hydroxide in potassium hydroxide

Elise Duquesne,[a,b] Stéphanie Betelu,[b*] Cyrille Bazin,[a] Alain Seron,[b] Ioannis Ignatiadis,[b] Hubert Perrot,[a] Ozlem Sel,[a] Catherine Debiemme-Chouvy,[a*]

[a] *Sorbonne Université, CNRS, Laboratoire Interfaces et Systèmes Électrochimiques, LISE, UMR 8235, 4 place Jussieu, 75005 Paris, France*

[b] *Bureau de Recherches Géologiques et Minières, 3 Avenue Claude Guillemin, 45100 Orléans, France*

ABSTRACT: The pseudo-capacitive properties and the mixed cation/anion-exchanger nature of layered double hydroxides (LDHs) were highlighted *via in situ* electrochemical and physicochemical analyses conducted in a KOH solution (1 mol/L) on a nano-Ni/Fe-LDH film. The reversible Ni(II)/Ni(III) oxidation/reduction reaction was monitored using an electrochemical quartz crystal microbalance (EQCM). The coupling of powerful electrochemical methods, EQCM and *ac*-electrogravimetry, and physicochemical techniques, EDX, XPS and *in situ* XRD, provided results clarifying the corresponding mass transfer mechanisms. *Ac*-electrogravimetry identified the nature, in terms of molar mass, kinetics and concentration variation of all reversibly transferred species associated with the redox reactions involving Ni and water molecules. This methodology demonstrated a reversible anion intercalation/de-intercalation into/from the interlayer spacing, in agreement with the redox reactions leading to modulate the electric charge of the layers. This phenomenon was also identified by *in situ* XRD. In addition, the variation of the pH at the LDH/electrolyte interface *via* a catalysed oxygen evolution reaction (OER) leads to cation electro-adsorption/desorption onto/from the external LDH surfaces.

INTRODUCTION

A layered double hydroxide (LDH) material consists of stacked brucite layers, positively charged due to the substitution of some divalent M^{II} cations by trivalent M^{III} cations. This excess of positive charges is compensated by the presence of exchangeable hydrated anions in the interlayer space[1], leading to the general formula $[M(II)_{1-x}M(III)_x(OH)_2]^{x+}(A^{n-}_{x/n}).mH_2O$.

Thus, LDHs have a high capacity for anion exchange (2-3 meq/g) comparable to that of anion exchange resins[2,3]. This renders them attractive for controlled anion release (drug delivery[4, 5], soil fertilizer[6]), anion containment (catalysis, anti-corrosion coating[7, 8]) and anion entrapment (water treatment[9]). Competition between anion species was first shown by Miyata[10] and fully described in other articles.[11,12,13]

Regarding applications in the field of energy storage or water treatment, the reversibility of ion transfer between an electrolyte and the basal space needs further investigation. Reversible ion transfer is controlled by tuning the oxidation state of metallic sites to generate a reversible modification of the positive charge excess within the layers. This phenomenon depends on the electrochemical accessibility of redox-active transition cations (ex: Co^{3+}/Co^{2+}, Ni^{3+}/Ni^{2+}, Fe^{3+}/Fe^{2+} etc.) that participate in an electron hopping mechanism.[14] The low electronic-conductivity performance of LDHs[15] is promoted by preparing thin LDH films coated on a working electrode surface (glassy carbon, platinum, gold, indium tin oxide…) by solvent casting, layer-by-layer assembly, or electrochemically assisted deposition.[14,1,16,17]

Several studies that explored reversible ion transfer phenomena related to the cyclic oxidation/reduction of electroactive cations within the layers.[1,18,19,20,21,22] showed the reversible intercalation of anions. Some also showed the contribution of cations,[1,18,20,22] and proposed assumptions concerning the nature of the species; one suggested the transfer of electrolytic cations,[20] another advanced anion intercalation/sorption influenced by electrolytic cations.[1] There is also evidence of the transfer of ion pairs,[22] or the loss of water molecules from the LDH interlayer space accompanied by a loss of protons from the LDH lattice.[18]

The redox reactivity of LDHs remains challenging to define, probably due to a duality of adsorption surface sites similar, by analogy, to cationic clay minerals.[23,24,25,26,27,28,29,30] Indeed, basal surfaces of cationic clay minerals have a permanent negative charge caused by isomorphic cationic substitution, whereas edge surfaces have a variable proton surface charge caused by functional hydroxyl groups. The redox reactions involving redox-active transition cations modulate the electric charge of the layers. For nontronite 2/1, the negative charge increase due to Fe(III) to Fe(II) reduction is balanced by the adsorption of cations into clay interlayers as well as by a specific sorption of protons from the solution. Prevalence of one compensating mechanism over another is related to the growing lattice distortion induced by Fe(III) reduction. At low reduction levels, interlayered cation adsorption dominates and some of the incorporated protons react with structural hydroxyl groups, leading to dehydroxylation of the structure.[31]

In addition, the reactivity of edge surfaces is strongly influenced by the net proton surface charge, which depends on pH and ionic strength, according to Brønsted–Lowry acid-base theory, through the following reactions:

$$\equiv M\text{-}OH + H^+ \leftrightarrows \equiv M\text{-}OH_2^+ \qquad \text{(R. 1)}$$

$$\equiv M\text{-}OH + OH^- \leftrightarrows \equiv M\text{-}O^- + H_2O \qquad \text{(R. 2)}$$

where M is a metal cation constituting the layered sheets and thus the clay edge surfaces. It implies the sorption of both cations and anions onto edge surfaces depending on the pH at the clay interface. In agreement with reaction 2, for pH >> pH_{PZNC} (point of zero net charge pH), the species $\equiv M\text{-}O^-$ predominates, leading to cation sorption onto edge surfaces.

By analogy to cationic clay minerals, the redox reactions involving structural-transition cations of the LDHs should modulate the positive electric charge of the layers, thus modulating the anionic transfer capacity and, to a lesser extent, the desorption of protons from structural OH groups to maintain electroneutrality. The reactivity of the edge surfaces and external basal sites should also be strongly influenced by the net proton surface charge.

To attribute the phenomena postulated by analogy with cationic clay minerals, the modification of the structural LDH charge via oxidation/reduction of part of the redox-active cations forming the layers should show the presence of anionic exchange sites. In addition, the use of a solution with a much higher pH than the pH_{PZNC} should allow identifying cation sorption which takes place on the LDH external basal sites and edge surfaces in agreement with the following reaction:

$$\equiv M\text{-}OH + OH^- + C^+ \leftrightarrows \equiv M\text{-}O\text{---}C + H_2O \qquad \text{(R. 2.1)}$$

where C^+ is a cation coming from the supporting electrolyte.

For this purpose, electrochemical techniques are well suited, as they allow redox transition of LDH electroactive cations as well as the modulation of interfacial pH via electro-catalytic properties of Ni/Fe LDHs *versus* water oxidation.[32,33,34, 35,36,37,38,39,40,41]

In addition, the *ac*-electrogravimetry method that combines measuring the electrochemical impedance (intensity/potential transfer function) and the mass/potential transfer function, will identify the reversibly exchanged species in terms of anions, cations or neutral species, as well as their molar mass, ease/difficulty of transfer, exchanged concentration and exchanged mass for each species at different potentials. This method was validated in studies of hydroxide[42] and oxide[43] materials and conductive polymers.[44] Our work provides new insight into the mechanisms of the interfacial redox reactions by exploiting *ac*-electrogravimetric methodology.

We paid special attention to Ni/Fe-LDH 6/2, known to be one of the most conductive LDHs whose electroactive Ni can be reversibly switched to the (+II) and (+III) oxidation states under polarization.[14] The use of nano-Ni/Fe-LDH 6/2 tends to enhance the number of transfer (intercalation and adsorption) sites onto both edge and basal surfaces. As Ni/Fe-LDH has a pH_{PZNC} of 8, this work was conducted in a KOH 1 mol/L solution whose pH value is higher than the pH_{PZNC}, in order to induce cationic sorption onto LDH border sites. The catalysed oxidation reaction of water[45,46,47,48] helped modulating the pH value at the LDH/electrolyte interface.

For the first time, we identified the nature of each reversibly transferred species (anions, cations and water molecules) related to redox reactions as well as determining the species kinetics. Energy-dispersive X-ray spectroscopy (EDX) and X-ray photoelectron spectroscopy (XPS) analyses confirmed the electro-sorption of cations, corroborating the pseudo-capacitive properties of a mixed cation/anion exchanger. The electro-catalytic properties of the interlayered water molecules were evidenced. In addition, *in situ* X-ray diffraction (XRD) analysis of LDH under polarization contributed to our understanding of LDH hydration during cyclic oxidation/reduction, investigating the transfer of water molecules from/to the interlayer space.

MATERIALS AND METHODS

(i) Synthesis of LDH by Co-Precipitation. LDH was synthesized with the varying-pH method[49] using bi-distilled water, $Ni(NO_3)_2.6H_2O$, $Fe(NO_3)_3.9H2O$, Na_2CO_3 (99.8% purity, Aldrich) and NaOH (98% purity, Aldrich) in air at 35°C. An aqueous salt solution with a molar ratio $Ni^{II}/Fe^{III} = 3$ was titrated with an alkaline aqueous solution containing 2.6 mol/L NaOH and 1 mol/L Na_2CO_3. This solution was introduced drop-by-drop with a peristaltic pump until the salt solution reached pH 10. The slurry was then stirred for 24 hrs at 60°C for maturation, which allowed the growth and crystallization of particles. To separate solids and residual solution, the slurry was centrifuged at 4000 rpm for five minutes. The supernatant was eliminated, and the final material underwent dialysis in de-ionized water equilibrated by atmospheric CO_2 renewed every day for five days to eliminate excess salts and allow NO_3^- to CO_3^{2-} anion exchange.

(ii) Physical and Chemical Definition of the Ni/Fe-LDH Powder. To allow a structural characterization of the material, part of the LDH powder was dried in a furnace at 70°C for 48 hr. This was studied by powder X-ray diffraction (PXRD) with a Panalytical Empyrean diffractometer, using Cu Kα radiation (λ=1.541 Å) operating at 45 kV and 40 mA at room temperature. The diffractometer is equipped

with a detector operating in scanning line mode using 255 channels. The scans were recorded from 4° to 84° (2θ) with a step of 0.026° and an acquisition time of 1200 seconds per step.

The morphology of the particles forming the powder and the cationic molar ratio were examined under an Ultra55 Zeiss field-emission-gun scanning electron microscope (FEG-SEM), operating at 10 kV. The anions intercalated in the interlayer space were identified by XPS analysis (Escalab 250xi, Thermo electron). The number of water molecules was determined by TGA analyses, done with a Mettler Toledo DSC1/ATG State instrument in the temperature range of 20-1000 °C, at a heating rate of 1 °C/min, under air atmosphere.

(iii) Preparation and Characterization of LDH Thin Films. Ethanol was added to the LDH slurry in order to avoid LDHs particles agglomeration during further drying process. A drop of the resulting suspension was deposited on the gold electrode of quartz resonators (A=0.2 cm^2, 9 MHz, AWS company, Spain) and the deposit was dried in air atmosphere. The LDH coating mass was then determined by quartz crystal microbalance (QCM) and its thickness was estimated by SEM.

(iv) *In situ* Coupled Electrochemical Analyses of the LDH

· *EQCM measurements.* EQCM measurements were performed in an aqueous solution of 1 mol/L KOH using a three-electrode cell connected to an Autolab potentiostat-galvanostat electrochemical work-station coupled with a lab-made QCM device. The counter electrode was a platinum grid, the reference electrode was a mercury/mercurous sulphate one, all the potentials were converted to the standard hydrogen electrode (SHE). The working electrode (WE) was a 9 MHz-gold patterned quartz substrate coated with a thin film of LDH. Cyclic electrogravimetric measurements were recorded at 10 mV/s over a potential window from 0.45 V to 0.71 V. Frequency changes (Δf) of the quartz crystal resonator were monitored simultaneously with the current (ΔI). The Δf was converted into the mass change (Δm) of the quartz crystal by applying the Sauerbrey equation: [50]

$$\Delta f = -\frac{2f_o^2}{A\sqrt{p_q \mu_q}} \Delta m \qquad \text{(Eq. 1)}$$

where A is the active surface of the gravimetric sensor, p_q is the quartz density, μ_q is the quartz shear modulus, and f_0 is the fundamental resonance frequency of the quartz.[51]

We note:

$$\Delta f = -C\,\Delta m \qquad \text{(Eq. 2)}$$

with C, the experimental sensitivity constant, 16.31 x 10^7 Hz g^{-1} cm^2 for 9 MHz.[51]

- *Ac-electrogravimetric measurements.* The *ac*-electrogravimetric setup was composed of a four-channel frequency response analyser (FRA, Solartron 1254) coupled to a lab-made potentiostat (SOTELEM-PGSTAT) and a lab-made QCM operating under dynamic regime.[52, 53] The WE was polarized at a chosen potential, to which a sinusoidal small-amplitude potential perturbation (80 mV rms) was superimposed. The microbalance frequency change (Δf) related to the mass response (Δm) of the modified WE was measured simultaneously with the current response (ΔI) of the electrochemical system. The resulting signals were sent to the four-channel FRA at the given potential and frequency modulation to obtain two main experimental transfer functions (TFs): electrogravimetric TF, $\left.\frac{\Delta m}{\Delta E}\right|_{exp}(\omega)$, and classical electrochemical impedance, $\left.\frac{\Delta E}{\Delta I}\right|_{exp}(\omega)$. The latter permits the experimental charge/potential transfer function $\left.\frac{\Delta q}{\Delta E}\right|_{exp}(\omega)$ to be obtained:

$$\left.\frac{\Delta q}{\Delta E}\right|_{\exp}(\omega) = \frac{1}{j\omega}\left.\frac{\Delta I}{\Delta E}\right|_{\exp}(\omega) \qquad \text{(Eq. 3)}$$

From the experimental electrogravimetric transfer function, $\left.\frac{\Delta m}{\Delta E}\right|_{exp}(\omega)$, experimental partial transfer functions can be calculated, eliminating the contribution of an anion or a cation, if three species are taken

into account: a cation (c), an anion (a) and solvent (s) (see SI file, part (iv) of *ac*-electrogravimetry theoretical part and data analysis). For example, if the contribution of the cation is extracted, the remaining experimental response of the anion and the solvent is calculated according to the following equation:

$$\left.\frac{\Delta m}{\Delta E}\right|_{\text{exp}}^{as}(\omega)=\left.\frac{\Delta m}{\Delta E}\right|_{\text{exp}}(\omega)+\frac{m_c}{F}\left.\frac{\Delta q}{\Delta E}\right|_{\text{exp}}(\omega) \qquad \text{(Eq. 4)}$$

In a similar manner, if the contribution of the anion is extracted, it becomes:

$$\left.\frac{\Delta m}{\Delta E}\right|_{\text{exp}}^{cs}(\omega)=\left.\frac{\Delta m}{\Delta E}\right|_{\text{exp}}(\omega)-\frac{m_a}{F}\left.\frac{\Delta q}{\Delta E}\right|_{\text{exp}}(\omega) \qquad \text{(Eq. 5)}$$

The experimental TFs given above were fitted with the theoretical expressions (see Supporting Information) defined in a model based on the interfacial flux of species under polarization using Mathcad Software version 15 (PTC). Fitting procedure provided parameters (K_i, G_i, $Rt_i = \frac{1}{FG_i}$, M_i and ΔC_i where i is an anion, cation or free solvent) regarding the nature of the species transferred, together with their interfacial dynamics and their concentration variation in the electrode (see Supporting Information).

***In situ* XRD measurements under polarization**

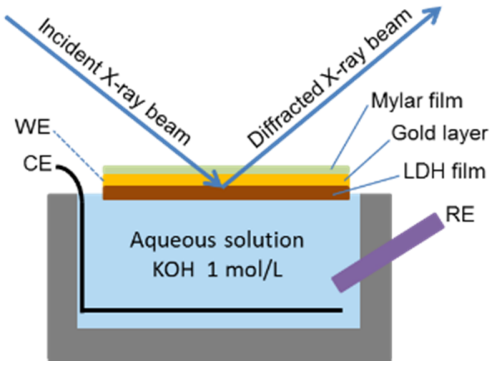

Figure 1. Scheme of *in situ* XRD analysis coupled with electrochemical measurements in KOH of a LDH thin film. WE: working electrode, CE: counter electrode and RE: reference electrode.

The reversible variation of the interlayer-distance period during the redox reaction of Ni was evaluated by *in situ* recording of the XRD characteristic 003-peak of the LDH. A working electrode made of mylar film (4.5 µm thick) coated with a 100 nm gold layer and a thin film of LDH was immersed in an aqueous KOH 1 mol/L solution (Figure 1). It underwent 40 polarization cycles to reflect the conditions of the *ac*-electrogravimetry experiments. The XRD measurements were recorded with a Panalytical Empyrean diffractometer operating at 45 kV and 40 mA at room temperature, under Cu Kα radiation (λ=1.541 Å) passing through a 15 mm mask with a 2° slit. Scans were recorded at 0.45 V (reduced state of LDH) and at 0.64 V (oxidized state of LDH) from 8° to 31° (2θ) with a step of 0.026° and a counting time of 600 s/step to follow the 003-peak of the LDH and a characteristic mylar peak taken as reference.

RESULTS

Physical and Chemical Characterization of Ni/Fe-LDH

PXRD analysis

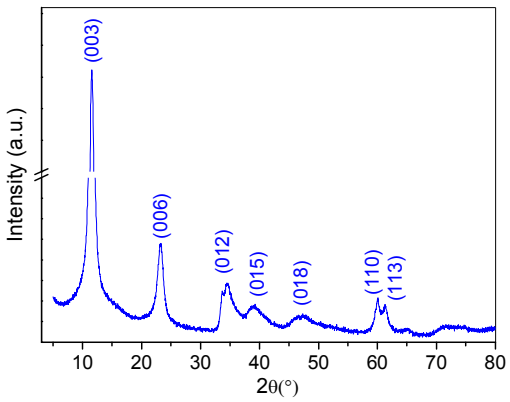

Figure 2. Powder XRD pattern of the Ni/Fe-LDH.

The powder XRD pattern of Ni/Fe-LDH (Figure 2) is characteristic of the LDH structure. The diffraction peaks were indexed to a hexagonal lattice of rhombohedral 3R symmetry[54] with three reflection groups:

(i) A set of basal (00l) reflections corresponds to structural stacking along the c-axis, allowing determination of the basal distance d (here 7.64 Å) that mainly depends upon the size of the intercalated species (anions and water molecules).[55] Parameter c of the lattice equals 3d (003) (here 22.92 Å).

(ii) The position of the (110) reflection is correlated to the lattice parameter a=2d (110) (here 3.08 Å), coinciding with the closest M–M distance in the brucite-like layers.

(iii) The positions of the (01l)/(10l) reflections common to hydrotalcite-like compounds, depending upon the polytype. These lattice parameters agree with those reported in the literature.[55]

FEG-SEM, EDX and XPS analyses.

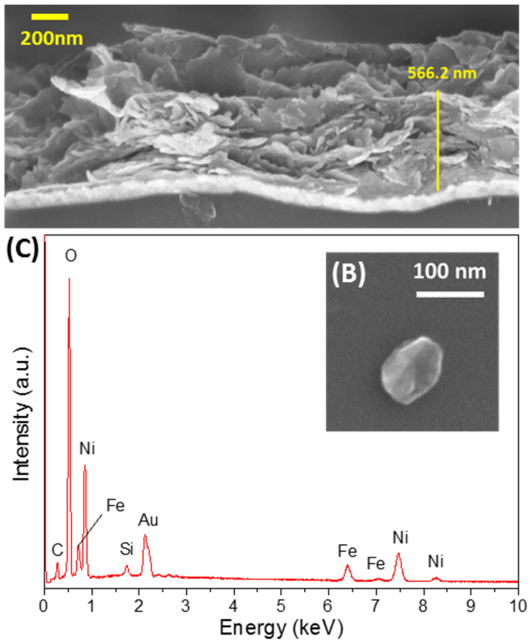

Figure 3. (A) FEG-SEM micrograph showing the cross-section of a gold-patterned quartz resonator modified with a thin LDH film, (B) FEG-SEM micrograph of a nanoplate of Ni/Fe-LDH 6/2 isolated on a silicon wafer, (C) EDX analysis of a thin film of Ni/Fe-LDH 6/2 deposited on the gold electrode of a quartz resonator.

FEG-SEM micrographs show that synthesized LDH consists of nanoplates with particle size about 80 nm (Figure 3B), agreeing with literature data.[49] The particle shown in Figure 3B is representative of the size distribution of the synthetized materials. The thickness of the film deposited onto the quartz resonator was measured by FEG-SEM (Figure 3A) at about 500 nm after deposition of 24.51 µg of dried LDH powder on a 0.2 cm^2 gold electrode.

A calibrated EDX analysis (Figure 3C) was done on a thin film of LDH dried on gold-coated quartz. The Ni/Fe cationic ratio was 76%/24% as expected during synthesis of the LDH.

An XPS survey spectrum (Figure S1) shows that no contribution around 400 eV was detected (N1s photopeak), confirming that no nitrate ions ~~were~~ was present in the LDH film after NO_3^- to CO_3^{2-} anion exchange under air atmospheric.

TGA Analysis. TG analysis (Figure S2) combined with calibrated EDX analysis allowed determination of the LDH chemical formula as $[Ni^{II}_{0.76}Fe^{III}_{0.24}(OH)_2(CO_3^{2-})_{0.12}]$. 0.5 H_2O. Therefore, an LDH coating of 24.51 µg —made by drop casting on the gold-coated quartz—consists of 0.227 10^{-6} mol LDH and thus of 1.04 10^{17} Ni sites. The anodic charge needed to oxidize all the Ni(II) into Ni(III) was thus 16.6 mC.

EQCM Study.

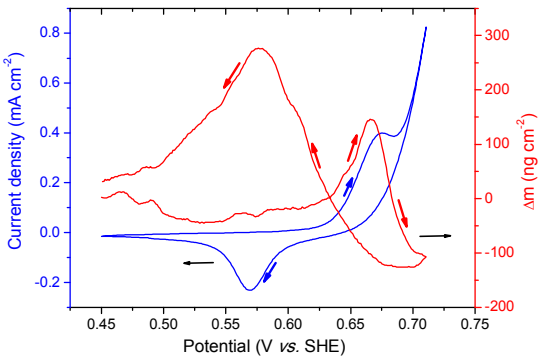

Figure 4. EQCM response during the 40th potential scan of a Ni/Fe-LDH coated quartz resonator in 1 mol/L KOH at a 10 mV/s potential scan rate.

First, thin films of Ni/Fe-LDH underwent 40 polarization cycles (from 0.45 V to 0.71 V at 10 mV/s) in an aqueous KOH solution of 1 mol/L at 10 mV/s. The current (I *vs*. E) and mass (m *vs*. E) responses were simultaneously recorded (Figure S3). After this preliminary treatment, reversibility of the mass variation was achieved (Figure S3). It is assumed that, during these 40 cycles, first interlayered carbonates were exchanged by hydroxyl ions (assuming that no water molecules are involved in the process 20% of the carbonates are exchanged) and then potassium cations were adsorbed onto the LDH external nanoplate surfaces (Figure S4A). Besides, the oxidation and reduction current peaks increased with the number of cycles (Figs. S3 and S4), indicating a rise in the number of redox-active Ni sites, probably due to some irreversibly oxidized Ni centres that enhance the material conductivity.[56,57,58,59]

Figure 4 shows the 40th cycle after which the system reached a steady state regarding both current and mass *versus* applied potential. A broad cathodic peak (at 0.570 V *vs*. SHE) and a broad anodic peak (at 0.674 V *vs.* SHE) respectively indicate the reduction and oxidation of Ni sites into the Brucite-like layer of LDH material.[14, 60]

The peak separation is 104 mV, comparable to the 98 mV value found in the literature[14] on platinum electrodes coated with Ni/Fe-LDH 6/2 denoting a slow-charge transfer. This phenomenon may be related to the known electronic transport within the LDH structure due to an electron hopping mechanism between adjacent nickel centres[61] although Fe also plays a role in this hopping process[14].

From the 40th potential cycle, the charge is estimated by integration of the cathodic peak to be 0.27 mC, corresponding to 1.685 x 10^{15} electroactive Ni atoms, or 1.62% of the Ni sites. Regarding the anodic peak, the concomitant Ni(II) and H_2O oxidation reactions do not allow an accurate determination of the percentage of formed Ni(III) sites (Figure S4b).

From the gravimetric response (Figure 4), it is obvious that the Ni/Fe-LDH film undergoes a mass increase followed by mass depletion during the anodic sweep, and a mass increase followed by a mass depletion during the cathodic sweep. According to the Ni(II) oxidation to Ni(III) within the LDH structure, the resulting modification in the redox state should induce OH^- intercalation within the interlayer space. In addition to and agreeing with the electrocatalytic behaviour of the Ni/Fe-LDH for OER, the resulting pH variations at the interface, from $pH >> pH_{PZNC}$ to $pH \approx pH_{PZNC}$, should induce modification of the charge at edge surfaces (Reaction (2.1)) and consequently in the electro-desorption/electrosorption of K^+ at external surfaces of the LDH nanosheets.

However, EQCM only provides an overview of the global transferred mass and cannot give precise information on the nature of the transferred species. It is challenging to deconvolute each species contribution into gravimetric and dynamic components with EQCM results, as the global cyclic electrogravimetry response is recorded at a certain scan rate, and at certain transfer kinetics.[62-64] Therefore, *ac*-electrogravimetric measurements were carried out for this purpose.

Ac-Electrogravimetric Investigations. After 40 potential cycles from 0.45 V to 0.71 V *vs.* SHE in KOH 1 mol/L, *ac*-electrogravimetry was carried out at different potentials, selected between the reduction and oxidation potentials of Ni (Figure 4), to gain insight into the (i) dynamic behaviour of each charged and uncharged species transfer at the interface, (ii) identification the nature of each transferred species, and (iii) evaluation of their respective concentration variation and kinetics as a function of the applied potential.

The data obtained at 0.65 V *vs.* SHE is shown in Figure 5. The charge/potential TF, $\left.\frac{\Delta q}{\Delta E}\right|_{\exp}(\omega)$ (derived from classical $\left.\frac{\Delta E}{\Delta I}\right|_{\exp}(\omega)$, Eq. 3) is given for a clear representation of the ionic transfer. The fitting of the experimental charge/potential transfer function was performed using the theoretical TF, $\left.\frac{\Delta q}{\Delta E}\right|_{th}^{global}(\omega)$ (Eq. SI-9). It

should be noted that at low frequencies the $\left.\frac{\Delta q}{\Delta E}\right|_{\exp}(\omega)$ TF contains the contribution from water oxidation reaction (see Figure S5) which also participates to the overall impedance with $Z_{par}(\omega)$ determined using Eq. SI-8. For the sake of clarity, this contribution was removed in order to visualize only the ionic contribution of the $\left.\frac{\Delta q}{\Delta E}\right|_{\exp}^{ion}(\omega)$ TF. The latter is fitted by using the theoretical expression given in Eq. SI-7. Both experimental and theoretical curves are shown in Figure 5A. A good agreement in terms of shape and frequencies is demonstrated.

Figure 5A shows two loops, one at high frequencies and another at low frequencies. They are attributed to the interfacial transfer of two different ionic species present in the electrolyte (Ion 1 and Ion 2). The kinetic parameter (K_i) (Eq. SI-3) and the parameter related to the ease/difficulty of interfacial transfer (G_i) (Eq. SI-4) for each ionic species were determined. This analysis permits to underline two ionic contributions, however, without any possibility to identify the involved ionic species at this step.

The same K_i and G_i values were then used in the fitting of the mass/potential transfer function, $\left.\frac{\Delta m}{\Delta E}\right|_{\exp}(\omega)$, by using the theoretical TF, $\left.\frac{\Delta m}{\Delta E}\right|_{th}(\omega)$, given in Eq. SI-14. Figure 5B evidences a first loop appearing in the third quadrant at high frequency. It is noted that a loop in the third quadrant is characteristic of cation contribution or free solvent molecules in the same flux direction.[52,53] Another contribution appears at intermediate frequencies in the third quadrant. Although small, a third contribution appears in the fourth quadrant at low frequency. Contributions in the fourth quadrant are characteristic of transfer of anions or of free solvent molecules in the same direction with the anions.

The fitting of the experimental data in Figure 5B evidences the nature of the three species, by the estimation of their atomic weight, m_i parameter in Eq. SI-14. K^+ (Ion 1 in Figure 5A) is transferred at high frequencies and OH^- (Ion 2 in Figure 5A) at low frequencies which confirms the configuration of two

ions determined by the $\left.\frac{\Delta q}{\Delta E}\right|_{\text{exp}}^{ion}(\omega)$ TF (Figure 5A, fitting of charge/potential transfer function using equation SI-7), water molecules are transferred in the same direction with the cations.

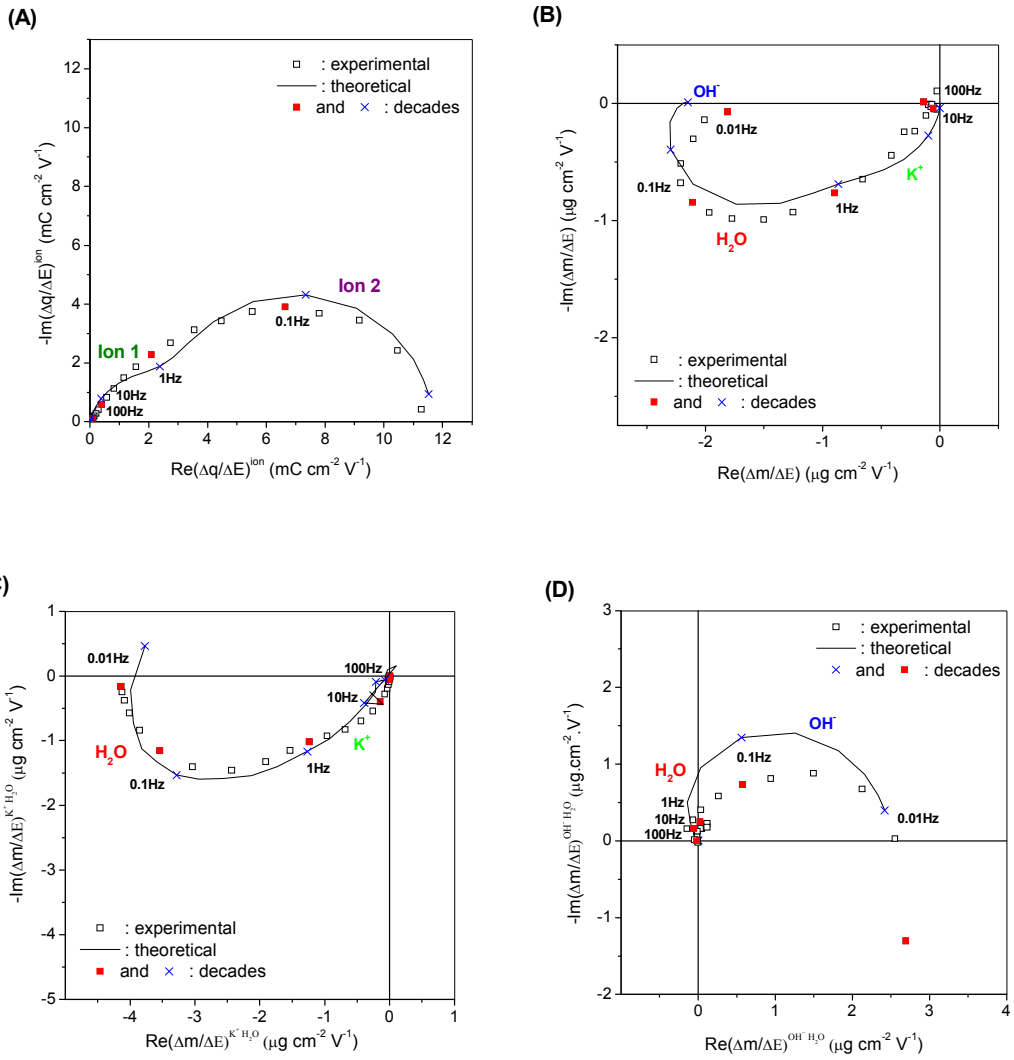

Figure 5. Experimental and fitted two main transfer functions (A) $(\Delta q/\Delta E)^{ion}(\omega)$ and (B) $(\Delta m/\Delta E)(\omega)$, and two partial transfer functions (C) $(\Delta m/\Delta E)^{K+,H2O}(\omega)$ and (D) $(\Delta m/\Delta E)^{OH-,H2O}(\omega)$. *Ac*-electrogravimetric measurements were performed on nano-Ni/Fe-LDH 6/2 in KOH 1 mol/L electrolyte at 0.65 V *vs*. SHE. Fitting parameters are presented in Table S1.

It is emphasized that before validating this multi-species contribution enlisted above, several other configurations were tested in the fitting of the experimental data using the theoretical functions in Eqs SI-6 and SI-16. The strict criteria for attaining a conclusive match between experimental and theoretical data must be fulfilled for all the TFs and for the so-called partial TFs obtained by removing the contribution of one of the species from the electrogravimetric TF, $\left.\frac{\Delta m}{\Delta E}\right|_{\exp}^{as}(\omega)$ and $\left.\frac{\Delta m}{\Delta E}\right|_{\exp}^{cs}(\omega)$ (Eqs 4 and 5, respectively), and analysing the residual response. The two experimental partial functions (Eqs 4 and 5) are fitted by the two theoretical partial TFs (Eqs SI-15 and SI-16) which resulted in a good agreement in terms of shape and frequencies (Figure 5C and Figure 5D). By this way, ambiguities concerning various possible models could be excluded, leading to the contributions of K^+, free solvent and OH^- as shown in Figure 5.

The same fitting procedure and validation control were used for all studied potentials from +0.575 V to +0.675 V, corresponding to the potential range where Ni oxidation and reduction reactions occur. The parameters K_i, G_i and $Rt_i = \frac{1}{FG_i}$ (Eq. SI-4) were estimated for all of them. Based on the K_i values (Figure 6A), the K^+ ion is the fastest of the three species exchanged at each potential, followed by H_2O and OH^-. The calculated Rt_i values (Eq. SI-4, Figure 6B) classify the transfer resistance of each species as follows: Rt_i (OH^-) > Rt_i (H_2O) ≥ Rt_i (K^+). This resistance of transfer is the highest for OH^- therefore its kinetics is the slowest. This finding is in good agreement with the intercalation process of OH^- into the LDH interlayer space. K^+ cations are faster and more easily transferred, especially at more anodic potentials (over 0.625 V vs. SHE), agreeing with the hypothesis of electro-adsorption onto more accessible sites like LDH edge surfaces. This will be discussed thereafter.

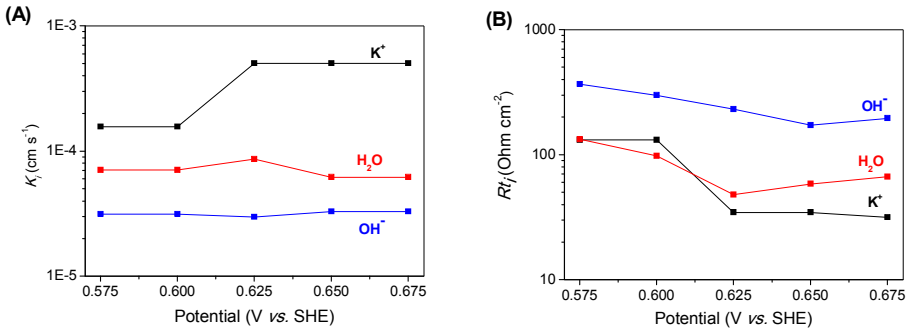

Figure 6. (A) Transfer kinetics rate, K_i, and (B) transfer resistance,Rt_i, of K^+, H_2O and OH^- as a function of applied potential in KOH 1 mol/L solution.

The evolutions of the relative concentration per unit volume, $C_i - C_o$, and the mass per area unit, m_i - m_0 were determined from the *ac*-electrogravimetric data in the potential range from 0.575 V to 0.675 V *vs*. SHE. The variation in concentration of the transferred species was estimated from the concentration/potential transfer function (Eq. SI-5) at low frequencies as shown below:[63]

$$\left.\frac{\Delta C_i}{\Delta E}\right|_{\omega \to 0} = \int_{E_0}^{E_1} -\frac{G_i}{K_i}\, dE \qquad \text{(Eq. 6)}$$

where E_0 and E_1 refer to two adjacent stationary potential values, at which the *ac*-electrogravimetry measurements have been performed. This concentration determination (Figure 7A), from 0.575 V to 0.675 V *vs.* SHE, showed that K^+ ions and H_2O molecules are transferred from the LDH to the electrolyte whereas OH^- ions are transferred from the electrolyte to the LDH when the Ni/Fe-LDH material is oxidized. The inverse processes occur during reduction.

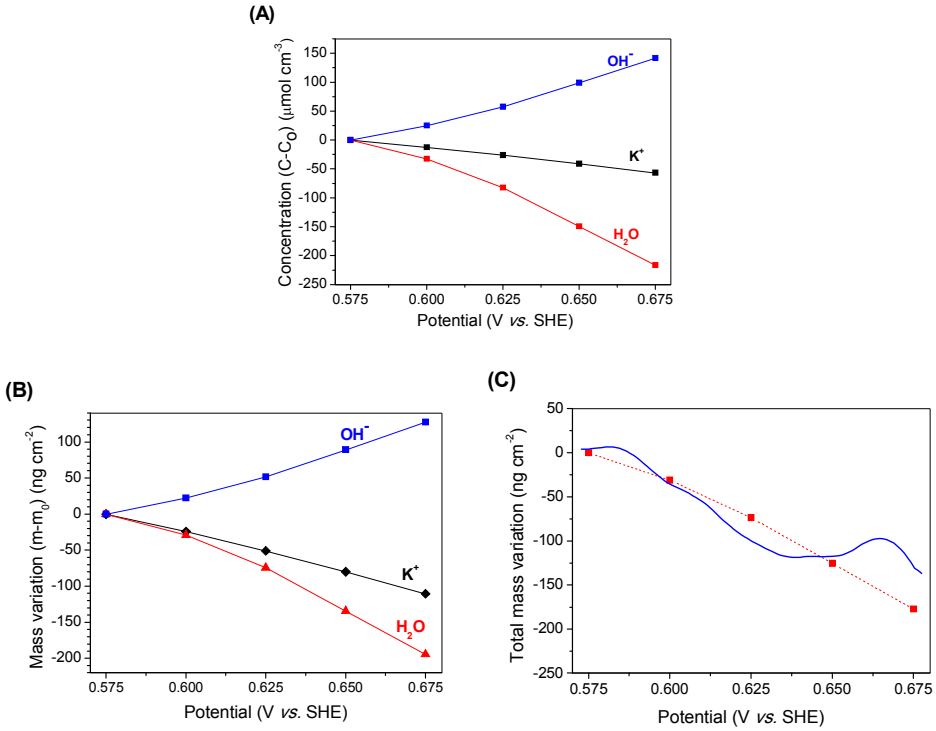

Figure 7. (A) Relative concentration change and (B) relative mass variation of K^+, H_2O and OH^- in the thin film of Ni/Fe-LDH as a function of the applied potential in KOH 1 mol/L solution, (C) comparison between the mass variation estimated with the *ac*-electrogravimetry (red squares) and that obtained directly from EQCM (10 mV/s) (full blue line).

From the $C_i - C_o$ values reported in Figure 7A, the mass variation per surface unit of each species for each potential can be calculated using equation 7:

$$m_i - m_0 = (C_i - C_o) M_i d_f \qquad \text{(Eq. 7)}$$

The results are reported in Figure 7B. The addition of these individual mass contributions leads to the "total mass variation re-calculated from the *ac*-electrogravimetry" (Figure 7C). Mass variations in the cathodic and anodic branches of classical EQCM response (Figure 4) were then averaged and compared

to the total exchanged mass found with the *ac*-electrogravimetry (Figure 7C). Both mass variations plotted in Figure 7C present the same behaviour with a change in the same order of magnitude. This finding evidences the accuracy of the developed model involving multi-species contribution with different proportion and time constants, at least for the studied potential range.

Note that for *ac*-electrogravimetry, a subsidiary irreversible reaction was considered for fitting of experimental data (Eqs SI-8 and SI-9). This side reaction was attributed to oxidation of the interlayered water molecules.

For a better insight regarding the sorption/interaction specific sites of each species identified (K^+, H_2O and OH^-), complementary analyses were performed on the Ni/Fe-LDH, *i.e.* EDX and XPS analyses and *in situ* XRD under LDH film polarization.

EDX and XPS Analysis.

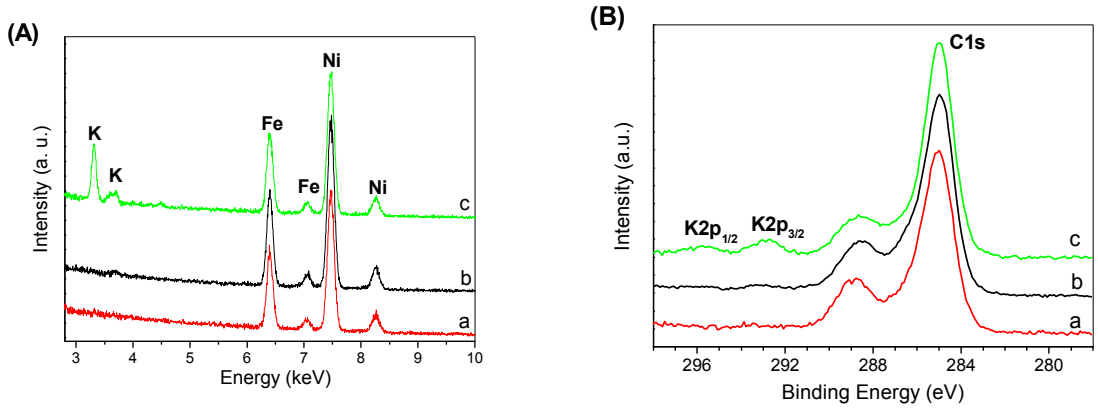

Figure 8. (A) EDX spectra; (B) K2p and C1s XPS spectra of (a) a thin film of dried LDH before immersion in KOH 1 mol/L, (b) after immersion in KOH 1 mol/L and (c) after immersion and polarization in KOH 1 mol/L.

Electrogravimetric results have shown the concomitant anion and cation transfer. The former was attributed to the species contributing to the charge compensation due to a redox process involving Ni and

the latter to a capacitive process. To confirm the electro-adsorption of cations (capacitive process) onto the LDH nanosheets, EDX and XPS analyses were done on a thin LDH film deposited on the gold electrode of a quartz resonator (i) before any experiment, (ii) after immersion in KOH 1 mol/L for 40 minutes (about the same duration as the 40 cycles) and (iii) after 40 polarization cycles from 0.45 V *vs*. SHE to 0.71 V *vs*. SHE at 10 mV/s in KOH 1 mol/L. Before EDX or XPS analyses, the LDH films in contact with KOH 1 mol/L were rinsed in NaOH 10^{-4} M to remove the KOH excess. The EDX and XPS spectra on Figure 8 do not show the presence of potassium ions in the LDH thin film either before or after 40 min immersion in KOH 1 mol/L without polarization. But potassium was detected by both EDX and XPS analyses in the film affected by 40 cycles of Ni oxidation/reduction in KOH 1 mol/L. These findings demonstrate the electro-adsorption of potassium cations.

In situ XRD Analysis.

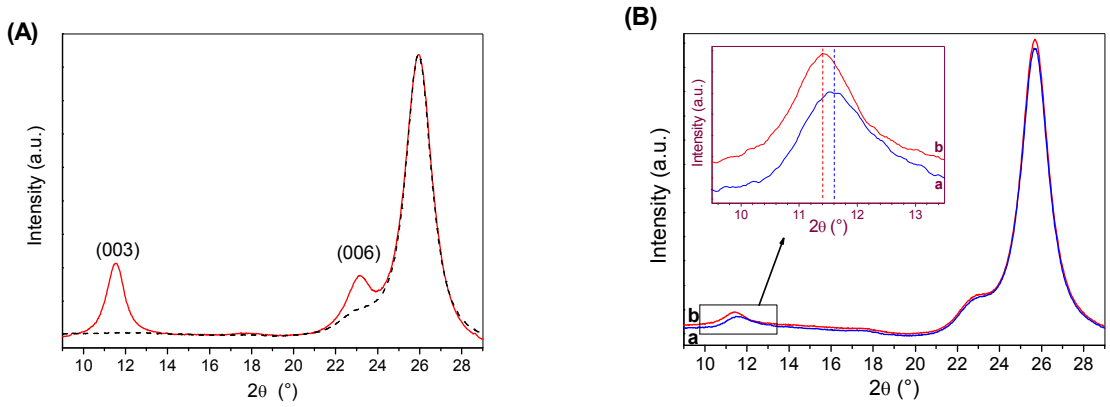

Figure 9. (A) XRD pattern of a mylar film coated with gold without (dashed line) and with (full line) a thin film of Ni/Fe-LDH. (B) *In situ* XRD patterns of a mylar film coated with gold and LDH under two polarizations: 0.450 V *vs.* SHE (red line, a) and 0.640 V *vs.* SHE (blue line, b). Insert: Magnification of the (003) peak under the two selected polarizations, 0.450 V *vs.* SHE (a) and 0.640 V *vs.* SHE (b).

For a better understanding of the influence of the electrochemical treatment undergone by LDH particles in aqueous KOH 1 mol/L, XRD analysis were done on LDH particles deposited on a gold-based electrode (Figure 1), consisting in a gold-coated mylar film. The experiments were run in the range from 9 to 29° in 2θ.

Analyses were first conducted on (i) gold-coated mylar film (Figure 9A, black dashed line) and (ii) dried LDH particles deposited on gold-coated mylar film (Figure 9A, red full line). The cubic[65] gold is illustrated by the small broad band at 2θ = 23° and the diffraction peaks at 2θ = 26°. The position of the (003) and (006) peaks of LDH is clearly seen around 11.5° and 23° (2θ), respectively.

Analyses were then conducted in KOH 1 mol/L solution after 40 polarization cycles, successively (i) at 0.640 V *vs*. SHE (oxidation of some Ni(II) sites, Figure 9B-a, blue line) and (ii) 0.450 V *vs.* SHE (reduction of Ni(III), Figure 9B-b, red line); these analyses were repeated five times. In the range from 22° to 24° in 2θ, the (006) peaks present a rather low signal-to-noise ratio due to the substrate (Figure 9A). The characteristic gold diffraction peak at 2θ = 26° remained in the same position regardless of the potential, and could be used as an internal reference for investigating the (003) LDH diffraction-peak behaviour; i.e. the evolution of basal distance versus applied potential.

Insert of Figure 9B shows the XRD spectrum between 9° and 15° in 2θ. Evaluation of the 003-period variation in solution is possible through the shift in position of the LDH (003) peak. Table 1 shows the shift in position of the 003-period for five successive experiments.

Table 1. **In situ DRX Measurements.**

Basal spacing obtained after five successive polarizations at 0.450 V (Ni(III) reduction) and at 0.640 V (Ni(II) oxidation) in KOH 1 mol/L.

Experiment number	Applied potential (V)	Basal spacing (Å)	Error (Å)	Basal spacing variation (Å)
1	0.450	7.4280	0.0239	---
2	0.640	7.3619	0.0444	-0.0661
3	0.450	7.4426	0.0250	0.0807
4	0.640	7.3855	0.0449	-0.0571
5	0.450	7.4532	0.0270	0.0677

The Ni oxidation at 0.640 V (experiments 2 and 4 in Table 1) leads to a decrease in the 003-period, whereas the Ni reduction at 0.450 V (experiments 3 and 5) leads to a 003-period increase. The redox reactions involve a local withdrawal/expansion of d-spacing from the average value.

DISCUSSION

Investigation of the electrochemical behaviour of nano-Ni/Fe-LDH 6/2 particles in KOH 1 mol/L through *ac*-electrogravimetry indicates pseudocapacitive LDH properties of a mixed cation and anion exchanger. Figure 10 summarizes all the steps and reactions occurring during the cycling potential imposed to the LDH film composed of nanosheets of Ni/Fe-LDH deposited on the Au electrode. Two different ionic species with different kinetics of transfer were detected, their contribution being attributed to a redox process due to Ni and a capacitive process ascribed to K^+. The later result is in good agreement with the results already reported on LDH[1] and LDH based structures[66,67].

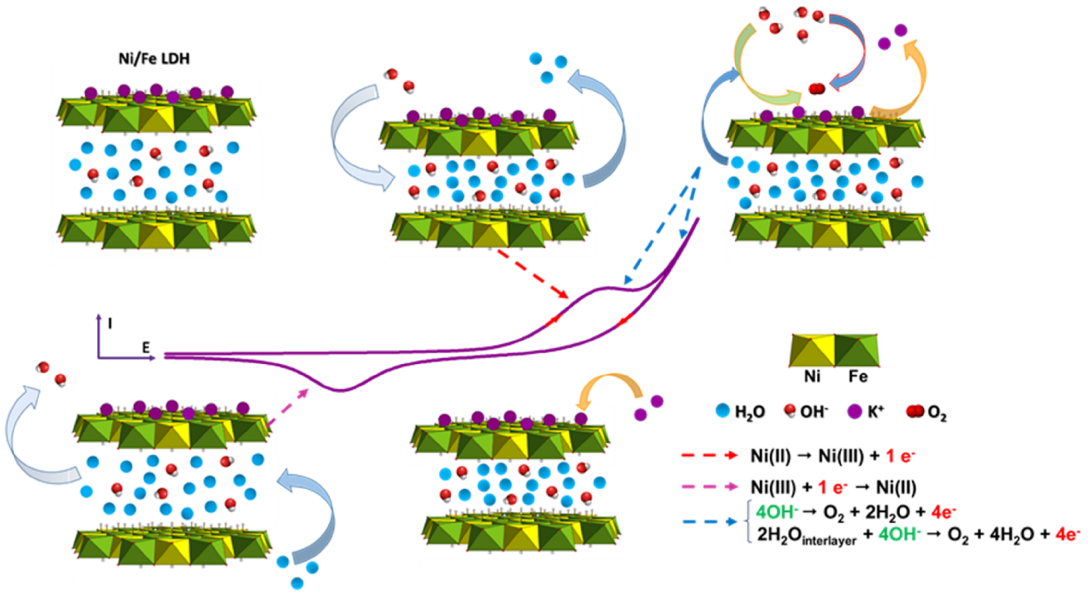

Figure 10. Scheme showing the various electron and species (ions and water) transfers during Ni/Fe polarization in KOH 1 mol/L.

Regarding the faradic process, the positive charge of the Brucite-like layer increases due to the oxidation of some Ni(II) sites to Ni(III); it is balanced by intercalation of OH^- anions in the LDH interlayer space. The intercalation of one OH^- anion and the expulsion of 1.5 interlayered water molecules are observed (Figure 7A) according to the following reaction:

$$[Ni^{II}_6Fe^{III}_2(OH)_{16-c}(OK)_c]^{2+}[(OH)_2]^{2-},4H_2O + x\ OH^- \leftrightarrows$$

$$[Ni^{II}_{6-x}Ni^{III}_xFe^{III}_2(OH)_{16-c}(OK)_c]^{(2+x)+}[(OH)_{2+x}]^{(2+x)-},(4-1.5x)\ H_2O + 1.5x\ H_2O + xe- \qquad \text{(R. 3)}$$

By analogy with observations on polymer films,[55] this phenomenon can be related to free water transfer caused by structural modifications of the electroactive film, leading to contraction of the LDH layer. EXAFS analysis of polarized Ni/Fe-LDH 6/2 electrodes indicates that both Ni–O and Fe–O distances decrease to ~1.9 Å (from d(Ni–O) = 2.06 Å and d(Fe–O) = 2.01 Å in an unpolarized electrode).[60] The Ni–O bond shortening is consistent with an increase in the Ni oxidation state.[68] Fe-bond contraction

is plausible as the lattice contraction accompanying Ni oxidation imposes a stronger ligand field on the Fe(III) centres, inducing crossover from a high-spin electronic structure to a low-spin state.[68] Fe–O distances of ~1.9 Å are consistent with low-spin Fe(III).[69]

Moreover, by analogy to cationic clay minerals, the nature and strength of the forces affecting a water molecule depend on its position within the pore space, here the distance to the LDH surfaces.[70] In clay minerals, crystalline swelling is controlled by a balance between strong attraction and repulsion[71,72] forces, and is more easily modelled by considering the potential energies of attraction and repulsion.[73] Again by analogy to cationic clay minerals, the potential attraction energy should be electrostatic, dominantly arising from Coulombic attraction between the positive surface-charge sites caused by isomorphous substitution and the negative charge of interlayer anions. Van der Waals interaction between adjacent layers may also contribute to the total potential attraction energy. The potential repulsion energy comes from the partial hydration potential energy of interlayer anions and, to a lesser degree, of positive surface-charge sites. By analogy to the swelling stages investigated by Lal and Shukla[74] the charge increase due to Ni(II) to Ni(III) oxidation reinforces Coulombic charges; the H_2O de-intercalation is opposed by the electrostatic attraction between anions and positively charged layers of the LDH. During the cathodic sweep, anion hydration is more important than the electroactive attraction between anions and the positively charged layer. In this way, *ac*-electrogravimetric measurements agree with *in situ* XRD under polarization. Redox reactions cause local withdrawal/expansion phenomena in agreement with the successive exclusion and insertion of interlayered water molecules in d spacing. By analogy to cationic clay minerals, these results confirm those provided by different authors.[75,76,77]

In situ XRD under polarization has especially contributed to our understanding of LDH hydration during cyclic oxidation/reduction. In addition, *ac*-electrogravimetric experiments revealed an irreversible

redox reaction that was attributed to the O_2 evolution reaction due to the oxidation of (i) interfacial OH^- and (ii) interlayered water molecules, for the latter according to the following reaction:

$$[Ni^{II}_{6-x}Ni^{III}_{x}Fe^{III}_{2}(OH)_{16-c}(OK)_c]^{(2+x)+}[(OH)_{2+x}]^{(2+x)-},(4-2x)H_2O + 2z\ OH^- \rightarrow$$

$$[Ni^{II}_{6-x}Ni^{III}_{x}Fe^{III}_{2}(OH)_{16-c}(OK)_c]^{(2+x)+}[(OH)_{2+x}]^{(2+x)-},(4-2x-z)H_2O + 2z\ H_2O + z/2\ O_2 + 2z\ e^- \quad \text{(R. 4)}$$

During the anodic sweep, the catalysed oxygen evolution reaction caused a decrease of the interfacial pH and allowed cation desorption from the negatively charged external surface of the LDH nanoplates. During the backward cathodic scan, the current cancelled and the interfacial pH became equal to that of the bulk solution, allowing cation sorption on the external negatively charged surface of the material. This phenomenon was confirmed by EDX and XPS analyses (K detection), in agreement with the following reaction:

$$[Ni^{II}_{6-x}Ni^{III}_{x}Fe^{III}_{2}(OH)_{16-c}(OH)_c]^{(2+x)+}[(OH)_{2+x}]^{(2+x)-},(4-2x-z)H_2O + c\ K^+ + c\ OH^- \leftrightarrows$$

$$[Ni^{II}_{6-x}Ni^{III}_{x}Fe^{III}_{2}(OH)_{16-c}(OK)_c]^{(2+x)+}[(OH)_{2+x}]^{(2+x)-},(4-2x-z)H_2O + c\ H_2O \quad \text{(R. 5)}$$

When the oxygen evolution reaction stops, water molecules should diffuse into the interlayer space of the Ni-Fe LDH.

Related to cation transfer, K^+ cations were shown to be faster and more easily transferred, especially at more anodic potentials, agreeing with the hypothesis of electro-adsorption onto more accessible sites like edge surfaces once the pH decreases and tends to the pH_{PZNC} value during the anodic sweep. Compared to cationic clay minerals whose edge surface can be reversibly deprotonated[29, 78], the positively charged LDH basal surface should render the H of the ≡M-OH groups more labile, which should be amplified by oxidation of the basal Ni(II). Thus, in the case of LDH, both edge surfaces and external basal surfaces are cation sorption sites.

CONCLUSIONS

For the first time, both electrochemical reactions and related ionic and water transfers in Ni/Fe-LDH 6/2 via electro-gravimetric definition were investigated. Experiments were conducted under polarization in KOH 1 mol/L, to differentiate the associated specific transfer sites, *i.e*. adsorption sites onto both edge and external basal surfaces, and intercalation sites in the interlayer space. For a better insight, complementary techniques included EDX and XPS analyses and *in-situ* XRD under polarization were performed.

Reversible Ni oxidation and reduction were observed using EQCM with a slow anion transfer. After 40 potential cycles, the film mass variation was reversible, regardless of complexity.

Ac-electrogravimetry identified the nature of the charged and uncharged species, as well as the kinetics rate ($K(K^+) > K(H_2O) > K(OH^-)$) and facility of transfer, exchanged concentration and exchanged mass for each species at different polarizations. It demonstrated the nano-Ni/Fe-LDH pseudocapacitive properties of a mixed cation (K^+) and anion (OH^-) exchanger. Ni redox reaction is responsible for anion intercalation/de-intercalation into/from the interlayer spacing. In the same time, the net swellability is determined by the balance achieved between modulated the positive layer charge and the negative charge of interlayer compensating anions. This mechanism was further demonstrated by *in-situ* XRD analyses. Concomitantly, the pH variation at the coated interface, due to a catalysed oxygen evolution reaction, caused cation electro-adsorption/desorption on the external surfaces. This was also confirmed by EDX and XPS analyses.

ASSOCIATED CONTENT

Supporting Information.

Ac-electrogravimetry theorical part and data analysis.

XPS survey spectrum, TGA curve, IV responses obtained during the 40 first potential cycles. Table showing the estimated values of parameters extracted from the fitting results of *ac*-electrogravimetry measurements. (PDF)

This material is available free of charge via the Internet at http://pubs.acs.org."

AUTHOR INFORMATION

Corresponding Authors

Stéphanie BETELU: s.betelu@brgm.fr

Catherine DEBIEMME-CHOUVY: catherine.debiemme-chouvy@sorbonne-universite.fr

ORCID

Stéphanie Betelu: 0000-0002-3050-1530

Catherine Debiemme-Chouvy: 0000-0001-7171-6039

Author Contributions

The manuscript was written through contributions of all authors. All authors have approved the final version of the manuscript.

Funding Sources

Financial support was provided by the BRGM and the Labex Matisse from Sorbonne University.

ACKNOWLEDGMENT

The authors thank Ms. Françoise Pillier for the SEM-FEG observations and Cédric Roosz for providing the schematic representation of the LDH structure. Dr H.M. Kluijver checked and edited the final English manuscript.

REFERENCES

1. Taviot-Gueho, C.; Vialat, P.; Leroux, F.; Razzaghi, F.; Perrot, H.; Sel, O.; Jensen, N. D.; Nielsen, U. G.; Peulon, S.; Elkaim, E.; Mousty, C., Dynamic Characterization of Inter- and Intralamellar Domains of Cobalt-Based Layered Double Hydroxides upon Electrochemical Oxidation. *Chemistry of Materials* **2016,** *28*, 7793-7806.

2. Cavani, F.; Trifiro, F.; Vaccari, A., Hydrotalcite-type anionic clays: preparation, properties and applications. *Catalysis Today* **1991,** *11*, 173-301.

3. Vaccari, A., Preparation and catalytic properties of cationic and anionic clays. *Catalysis Today* **1998,** *41*, 53-71.

4. Cao, Z.; Li, B.; Sun, L.; Li, L.; Xu, Z. P.; Gu, Z., 2D Layered Double Hydroxide Nanoparticles: Recent Progress toward Preclinical/Clinical Nanomedicine. *Small Methods* **2019**, 1900343.

5. Arrabito, G.; Bonasera, A.; Prestopino, G.; Orsini, A.; Mattoccia, A.; Martinelli, E.; Pignataro, B.; Medaglia, P. G., Layered Double Hydroxides: A Toolbox for Chemistry and Biology. *Crystals* **2019,** *9*, 361.

6. Bernardo, M. P.; Guimaraes, G. G. F.; Majaron, V. F.; Ribeiro, C., Controlled Release of Phosphate from Layered Double Hydroxide Structures: Dynamics in Soil and Application as Smart Fertilizer. *Acs Sustainable Chemistry & Engineering* **2018,** *6*, 5152-5161.

7. Dennis, R. V.; Patil, V.; Andrews, J. L.; Aldinger, J. P.; Yadav, G. D.; Banerjee, S., Hybrid nanostructured coatings for corrosion protection of base metals: a sustainability perspective. *Materials Research Express* **2015,** *2*, 032001.

8. Guo, L.; Wu, W.; Zhou, Y.; Zhang, F.; Zeng, R.; Zeng, J., Layered double hydroxide coatings on magnesium alloys: A review. *Journal of Materials Science & Technology* **2018,** *34*, 1455-1466.

9. Zumreoglu-Karan, B.; Ay, A. N., Layered double hydroxides - multifunctional nanomaterials. *Chemical Papers* **2012,** *66*, 1-10.

10. Miyata, S., Anion exchange properties of hydrotalcite-like compounds. *Clays and Clay Minerals* **1983,** *31*, 305-311.

11. Goh, K. H.; Lim, T. T.; Dong, Z., Application of layered double hydroxides for removal of oxyanions: A review. *Water Research* **2008,** *42*, 1343-1368.

12. Delorme, F.; Seron, A.; Vergnaud, B.; Galle-Cavalloni, P.; Jean-Prost, V.; Manguin, J., Evidence of the influence of the cationic composition on the anionic affinity of layered double hydroxides. *Journal of Materials Science* **2013,** *48*, 5273-5279.

13. Ardau, C.; Frau, F.; Lattanzi, P., New data on arsenic sorption properties of Zn-Al sulphate layered double hydroxides: Influence of competition with other anions. *Applied Clay Science* **2013,** *80-81*, 1-9.

14. Scavetta, E.; Vlamidis, Y.; Posati, T.; Nocchetti, M.; Tonelli, D., Effect of the Synthesis Route and Fe Presence on the Redox Activity of Ni in Layered Double Hydroxides. *Chemelectrochem* **2016,** *3*, 1320-1328.

15. Lal, M.; Howe, A. T., Studies of zinc-chromium hydroxy salts. 2. Composite anion conductors of pressed disks of $Zn_2Cr(OH)_6X.nH_2O$, where X^- = F^-, Cl^-, Br^-,I^-, NO_3^- and 1/2 CO_3^{2-}. *Journal of Solid State Chemistry* **1981,** *39*, 377-386.

16. Xu, L.; Lin, Y. Q.; Chen, X.; Lu, Y. L.; Yang, W. S., Electrodeposition of Platinum Nanoparticles on MgAl-layered Double Hydroxide Modified Indium Tin Oxide Electrode for Electrochemical Glucose Biosensor. *Chemical Journal of Chinese Universities-Chinese* **2016,** *37*, 442-447.

17. Desigaux, L.; Ben Belkacem, M.; Richard, P.; Cellier, J.; Leone, P.; Cario, L.; Leroux, F.; Taviot-Gueho, C.; Pitard, B., Self-assembly and characterization of layered double hydroxide/DNA hybrids. *Nano Letters* **2006,** *6*, 199-204.

18. Roto, R.; Yamagishi, A.; Villemure, G., Electrochemical quartz crystal microbalance study of mass transport in thin film of a redox active Ni-Al-Cl layered double hydroxide. *Journal of Electroanalytical Chemistry* **2004,** *572*, 101-108.

19. Scavetta, E.; Ballarin, B.; Corticelli, C.; Gualandi, I.; Tonelli, D.; Prevot, V.; Forano, C.; Mousty, C., An insight into the electrochemical behavior of Co/Al layered double hydroxide thin films prepared by electrodeposition. *Journal of Power Sources* **2012,** *201*, 360-367.

20. Roto, R.; Villemure, G., Mass transport in thin films of $Fe(CN)_6^{4-}$ exchanged Ni-Al layered double hydroxide monitored with an electrochemical quartz crystal microbalance. *Journal of Electroanalytical Chemistry* **2006,** *588*, 140-146.

21. Guo, X. X.; Zhang, F. Z.; Evans, D. G.; Duan, X., Layered double hydroxide films: synthesis, properties and applications. *Chemical Communications* **2010,** *46*, 5197-5210.

22. Su, L. H.; Zhang, X. G.; Mi, C. H.; Liu, Y., Insights into the electrochemistry of layered double hydroxide containing cobalt and aluminum elements in lithium hydroxide aqueous solution. *Journal of Power Sources* **2008,** *179*, 388-394.

23. Bradbury, M. H.; Baeyens, B., A mechanistic description of Ni and Zn sorption on Na-montmorillonite .2. Modelling. *Journal of Contaminant Hydrology* **1997,** *27*, 223-248.

24. Bradbury, M. H.; Baeyens, B., Modelling the sorption of Zn and Ni on Ca-montmorillonite. *Geochimica Et Cosmochimica Acta* **1999,** *63*, 325-336.

25. Avena, M. J.; De Pauli, C. P., Proton adsorption and electrokinetics of an Argentinean montmorillonite. *Journal of Colloid and Interface Science* **1998,** *202*, 195-204.

26. Tombacz, E.; Szekeres, M., Colloidal behavior of aqueous montmorillonite suspensions: the specific role of pH in the presence of indifferent electrolytes. *Applied Clay Science* **2004,** *27*, 75-94.

27. Tournassat, C.; Ferrage, E.; Poinsignon, C.; Charlet, L., The titration of clay minerals II. Structure-based model and implications for clay reactivity. *Journal of Colloid and Interface Science* **2004,** *273*, 234-246.

28. Tournassat, C.; Neaman, A.; Villieras, F.; Bosbach, D.; Charlet, L., Nanomorphology of montmorillonite particles: Estimation of the clay edge sorption site density by low-pressure gas adsorption and AFM observations. *American Mineralogist* **2003,** *88*, 1989-1995.

29. Tournassat, C.; Davis, J. A.; Chiaberge, C.; Grangeon, S.; Bourg, I. C., Modeling the Acid-Base Properties of Montmorillonite Edge Surfaces. *Environmental Science & Technology* **2016,** *50*, 13436-13445.

30. Tournassat, C.; Bizi, M.; Braibant, G.; Crouzet, C., Influence of montmorillonite tactoid size on Na-Ca cation exchange reactions. *Journal of Colloid and Interface Science* **2011,** *364*, 443-454.

31. Hadi, J.; Tournassat, C.; Ignatiadis, I.; Greneche, J. M.; Charlet, L., Modelling CEC variations versus structural iron reduction levels in dioctahedral smectites. Existing approaches, new data and model refinements. *Journal of Colloid and Interface Science* **2013,** *407*, 397-409.

32. Song, F.; Hu, X. L., Exfoliation of layered double hydroxides for enhanced oxygen evolution catalysis. *Nature Communications* **2014,** *5*.

33. Gong, M.; Li, Y. G.; Wang, H. L.; Liang, Y. Y.; Wu, J. Z.; Zhou, J. G.; Wang, J.; Regier, T.; Wei, F.; Dai, H. J., An Advanced Ni-Fe Layered Double Hydroxide Electrocatalyst for Water Oxidation. *Journal of the American Chemical Society* **2013,** *135*, 8452-8455.

34. Lee, Y.; Choi, J. H.; Jeon, H. J.; Choi, K. M.; Lee, J. W.; Kang, J. K., Titanium-embedded layered double hydroxides as highly efficient water oxidation photocatalysts under visible light. *Energy & Environmental Science* **2011,** *4*, 914-920.

35. Zhang, J. F.; Liu, J. Y.; Xi, L. F.; Yu, Y. F.; Chen, N.; Sun, S. H.; Wang, W. C.; Lange, K. M.; Zhang, B., Single-Atom Au/NiFe Layered Double Hydroxide Electrocatalyst: Probing the Origin of Activity for Oxygen Evolution Reaction. *Journal of the American Chemical Society* **2018,** *140*, 3876-3879.

36. Morales-Guio, C. G.; Mayer, M. T.; Yella, A.; Tilley, S. D.; Gratzel, M.; Hu, X. L., An Optically Transparent Iron Nickel Oxide Catalyst for Solar Water Splitting. *Journal of the American Chemical Society* **2015,** *137*, 9927-9936.

37. Hunter, B. M.; Blakemore, J. D.; Deimund, M.; Gray, H. B.; Winkler, J. R.; Muller, A. M., Highly Active Mixed-Metal Nanosheet Water Oxidation Catalysts Made by Pulsed-Laser Ablation in Liquids. *Journal of the American Chemical Society* **2014,** *136*, 13118-13121.

38. Ahn, H. S.; Bard, A. J., Surface Interrogation Scanning Electrochemical Microscopy of Ni1-xFexOOH (0 < x < 0.27) Oxygen Evolving Catalyst: Kinetics of the "fast" Iron Sites. *Journal of the American Chemical Society* **2016,** *138*, 313-318.

39. Gorlin, M.; Chernev, P.; de Araujo, J. F.; Reier, T.; Dresp, S.; Paul, B.; Krahnert, R.; Dau, H.; Strasser, P., Oxygen Evolution Reaction Dynamics, Faradaic Charge Efficiency, and the Active Metal Redox States of Ni-Fe Oxide Water Splitting Electrocatalysts. *Journal of the American Chemical Society* **2016,** *138*, 5603-5614.

40. Dong, Y.; Zhang, P. X.; Kou, Y. L.; Yang, Z. Y.; Li, Y. P.; Sun, X. M., A First-Principles Study of Oxygen Formation Over NiFe-Layered Double Hydroxides Surface. *Catalysis Letters* **2015,** *145*, 1541-1548.

41. Cai, Z. Y.; Bu, X. M.; Wang, P.; Ho, J. C.; Yang, J. H.; Wang, X. Y., Recent advances in layered double hydroxide electrocatalysts for the oxygen evolution reaction. *Journal of Materials Chemistry A* **2019,** *7*, 5069-5089.

42. Bernard, P.; Gabrielli, C.; Keddam, M.; Takenouti, H.; Leonardi, J.; Blanchard, P., *Ac* quartz crystal microbalance applied to the studies of the nickel-hydroxide behavior in alkaline-solutions. *Electrochimica Acta* **1991,** *36*, 743-746.

43. Benmouhoub, C.; Agrisuelas, J.; Benbrahim, N.; Pillier, F.; Gabrielli, C.; Kadri, A.; Pailleret, A.; Perrot, H.; Sel, O., Influence of the Incorporation of CeO_2 Nanoparticles on the Ion Exchange Behavior of Dodecylsulfate Doped Polypyrrole Films: Ac-Electrogravimetry Investigations. *Electrochimica Acta* **2014,** *145*, 270-280.

44. Gao, W. L.; Sel, O.; Perrot, H., Electrochemical and viscoelastic evolution of dodecyl sulfate-doped polypyrrole films during electrochemical cycling. *Electrochimica Acta* **2017,** *233*, 262-273.

45. Trotochaud, L.; Young, S. L.; Ranney, J. K.; Boettcher, S. W., Nickel-Iron Oxyhydroxide Oxygen-Evolution Electrocatalysts: The Role of Intentional and Incidental Iron Incorporation. *Journal of the American Chemical Society* **2014,** *136*, 6744-6753.

46. Corrigan, D. A., The catalysis of the oxygen evolution recation by iron impurities in thin-film nickel-oxide electrodes. *Journal of the Electrochemical Society* **1987,** *134*, 377-384.

47. Stevens, M. B.; Trang, C. D. M.; Enman, L. J.; Deng, J.; Boettcher, S. W., Reactive Fe-Sites in Ni/Fe (Oxy)hydroxide Are Responsible for Exceptional Oxygen Electrocatalysis Activity. *Journal of the American Chemical Society* **2017,** *139*, 11361-11364.

48. Gao, X. Y.; Pan, X. Y.; Long, X.; Yi, Z. G., Room-Temperature Synthesis FeNiCo Layered Double Hydroxide as an Excellent Electrochemical Water Oxidation Catalyst. *Journal of the Electrochemical Society* **2017,** *164*, II755-II759.

49. Seron, A.; Delorme, F., Synthesis of layered double hydroxides (LDHs) with varying pH: A valuable contribution to the study of Mg/Al LDH formation mechanism. *Journal of Physics and Chemistry of Solids* **2008,** *69*, 1088-1090.

50. Sauerbrey, G., Verwendung von schwingquarzen zur wagung dunner schichten und zur mikrowagung. *Zeitschrift Fur Physik* **1959,** *155*, 206-222.

51. Bizet, K.; Gabrielli, C.; Perrot, H., Immunodetection by quartz crystal microbalance - A new approach for direct detection of rabbit IgG and peroxidase. *Applied Biochemistry and Biotechnology* **2000,** *89*, 139-149.

52. Gabrielli, C.; Garcia-Jareno, J. J.; Keddam, M.; Perrot, H.; Vicente, F., Ac-electrogravimetry study of electroactive thin films. I. Application to Prussian Blue. *Journal of Physical Chemistry B* **2002,** *106*, 3182-3191.

53. Gabrielli, C.; Garcia-Jareno, J. J.; Keddam, M.; Perrot, H.; Vicente, F., Ac-electrogravimetry study of electroactive thin films. II. Application to polypyrrole. *Journal of Physical Chemistry B* **2002,** *106*, 3192-3201.

54. Hunter, B.; Winkler, J.; Gray, H.; Mueller, A., Effect of interlayer anions on NiFe -LDH nanosheet water oxidation activity. *Abstracts of Papers of the American Chemical Society* **2016,** *251*, 1.

55. Bookin, A. S.; Cherkashin, V. I.; Drits, V. A., Reinterpretation of the X-ray-diffraction patterns of stichtite and reevesite. *Clays and Clay Minerals* **1993,** *41*, 631-634.

56. Qiu, J. B.; Villemure, G., Anionic clay-modified electrodes - Electrochemical activity of nickel(II) sites in layered double hydroxide films. *Journal of Electroanalytical Chemistry* **1995,** *395*, 159-166.

57. Qiu, J. B.; Villemure, G., Anionic clay modified electrodes: Electron transfer mediated by electroactive nickel, cobalt or manganese sites in layered double hydroxide films. *Journal of Electroanalytical Chemistry* **1997,** *428*, 165-172.

58. Corrigan, D. A.; Bendert, R. M., Effect of coprecipitated metal-ions on the electrochemistry of nickel-hydroxide thin-films - cyclic voltammetry in 1M KOH. *Journal of the Electrochemical Society* **1989,** *136*, 723-728.

59. Song, F.; Hu, X. L., Exfoliation of layered double hydroxides for enhanced oxygen evolution catalysis. *Nature Communications* **2014,** *5*, 4477.

60. Friebel, D.; Louie, M. W.; Bajdich, M.; Sanwald, K. E.; Cai, Y.; Wise, A. M.; Cheng, M. J.; Sokaras, D.; Weng, T. C.; Alonso-Mori, R.; Davis, R. C.; Bargar, J. R.; Norskov, J. K.; Nilsson, A.; Bell, A. T., Identification of Highly Active Fe Sites in (Ni,Fe)OOH for Electrocatalytic Water Splitting. *Journal of the American Chemical Society* **2015,** *137*, 1305-1313.

61. Scavetta, E.; Berrettoni, M.; Giorgetti, M.; Tonelli, D., Electrochemical characterisation of Ni/Al-X hydrotalcites and their electrocatalytic behaviour. *Electrochimica Acta* **2002,** *47*, 2451-2461.

62. Arias, C. R.; Debiemme-Chouvy, C.; Gabrielli, C.; Laberty-Robert, C.; Pailleret, A.; Perrot, H.; Sel, O., New Insights into Pseudocapacitive Charge-Storage Mechanisms in Li-Birnessite Type MnO_2 Monitored by Fast Quartz Crystal Microbalance Methods. *Journal of Physical Chemistry C* **2014,** *118*, 26551-26559.

63. Escobar-Teran, F.; Arnau, A.; Garcia, J. V.; Jimenez, Y.; Perrot, H.; Sel, O., Gravimetric and dynamic deconvolution of global EQCM response of carbon nanotube based electrodes by Ac-electrogravimetry. *Electrochemistry Communications* **2016,** *70*, 73-77.

64. Goubaa, H.; Escobar-Teran, F.; Ressam, I.; Gao, W.; El Kadib, A.; Lucas, I. T.; Raihane, M.; Lahcini, M.; Perrot, H.; Sel, O., Dynamic Resolution of Ion Transfer in Electrochemically Reduced Graphene Oxides Revealed by Electrogravimetric Impedance. *Journal of Physical Chemistry C* **2017,** *121,* 9370-9380.

65. Jaffee, R. I.; Smith, E. M.; Gonser, B. W., The constitution of the gold germanium system. *Transactions of the American Institute of Mining and Metallurgical Engineers* **1945,** *161*, 366-372.

66. Kim, M. S.; Kim, K. B., A study on the phase transformation of electrochemically precipitated nickel hydroxides using an electrochemical quartz crystal microbalance. *Journal of the Electrochemical Society* **1998,** *145*, 507-511.

67. Wehrens-Dijksma, M.; Notten, P. H. L., Electrochemical Quartz Microbalance characterization of $Ni(OH)_2$-based thin film electrodes. *Electrochimica Acta* **2006,** *51*, 3609-3621.

68. Hunter, B. M.; Winkler, J. R.; Gray, H. B., Iron Is the Active Site in Nickel/Iron Water Oxidation Electrocatalysts. *Molecules* **2018,** *23*, 903.

69. Sanson, A.; Kantor, I.; Cerantola, V.; Irifune, T.; Carnera, A.; Pascarelli, S., Local structure and spin transition in Fe_2O_3 hematite at high pressure. *Physical Review B* **2016,** *94*, 014112.

70. Likos, W. J.; Lu, N., Pore-scale analysis of bulk volume change from crystalline interlayer swelling in Na^+- and Ca^{2+}-smectite. *Clays and Clay Minerals* **2006,** *54*, 515-528.

71. Kittrick, J. A., Interlayer forces in montmorillonite and vermiculite. *Soil Science Society of America Proceedings* **1969,** *33*, 217-222.

72. Norrish, K., The swelling of montmorillonite. *Discussions of the Faraday Society* **1954,** *18*, 120-134.

73. Laird, D. A., Model for crystalline swelling of 2:1 phyllosilicates. *Clays and Clay Minerals* **1996,** *44*, 553-559.

74. Rattan, L.; K., S. M., *Principle of soil Physics*. Marcel Dekker: New York, 2004.

75. Stucki, J. W.; Low, P. F.; Roth, C. B.; Golden, D. C., Effects of oxidation-state of octahedral iron on clay swelling. *Clays and Clay Minerals* **1984,** *32* (5), 357-362.

76. Wu, J.; Low, P. F.; Roth, C. B., Effects of octahedral-iron reduction and swelling pressure on interlayer distances in Na-nontronite. *Clays and Clay Minerals* **1989,** *37*, 211-218.

77. Stucki, J. W.; Lee, K.; Zhang, L. Z.; Larson, R. A., Effects of iron oxidation state on the surface and structural properties of smectites. *Pure and Applied Chemistry* **2002,** *74*, 2145-2158.

78. Secor, R. B.; Radke, C. J., Spillover of the diffuse double-layer on montmorillonite particles. *Journal of Colloid and Interface Science* **1985,** *103*, 237-244.

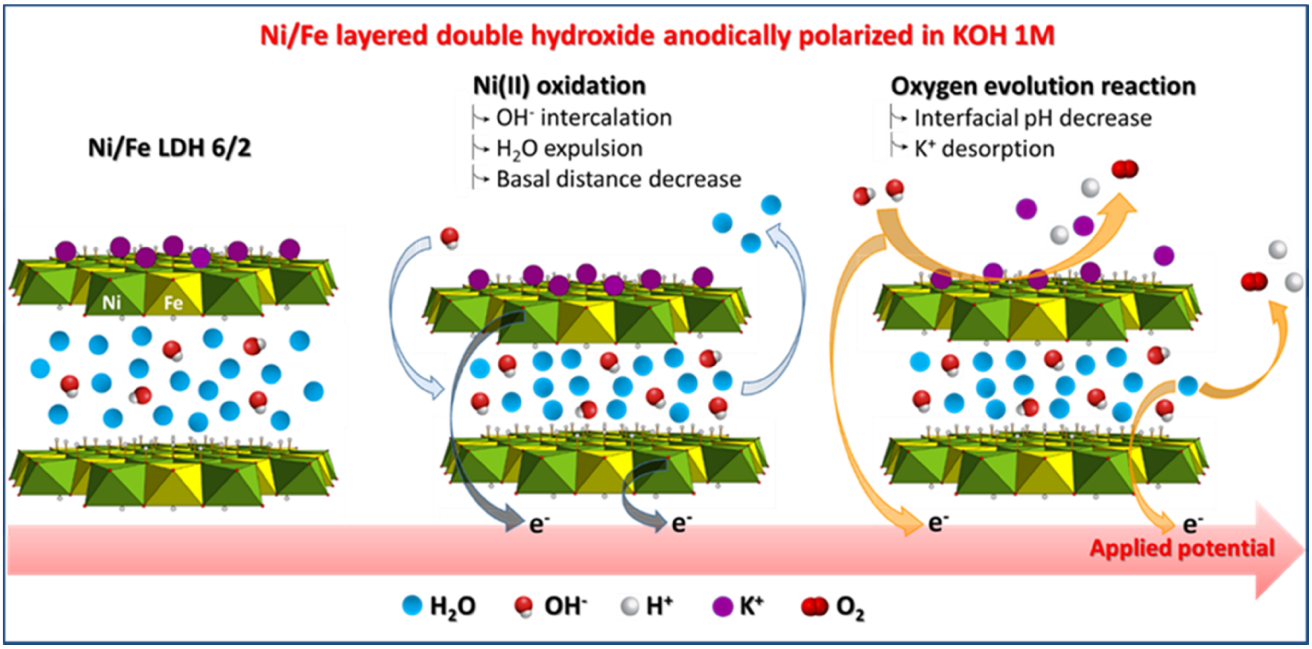
Ni/Fe layered double hydroxide anodically polarized in KOH 1M
Ni/Fe LDH 6/2
Ni(II) oxidation
OH- intercalation
H2O expulsion
Basal distance decrease
Oxygen evolution reaction
Interfacial pH decrease
K+ desorption
Ni
Fe
e-
e-
e-
e-
Applied potential
H2O
OH-
H+
K+
O2